Supporting Information

Molecular dynamics simulations of water sorption in a perfluorosulfonic acid membrane

Kevin B. Daly, Jay B. Benziger, Pablo G. Debenedetti, and Athanassios Z. Panagiotopoulos

Department of Chemical and Biological Engineering, Princeton University, Princeton, New Jersey 08544

S1 Force Field

S1.1 Definitions of particle types

The particle types in the Nafion side and backbone are defined in Figure S1. In addition, the CF_3 groups at the chain ends are of type "CF3". Water molecules consist of three particle types: "OWT4", "HW", and "IW", corresponding to the oxygen atom, hydrogen atoms, and virtual site, respectively. Hydronium molecules consist of two particle types: "ON" and "HN", corresponding to the oxygen and hydrogen atoms, respectively.

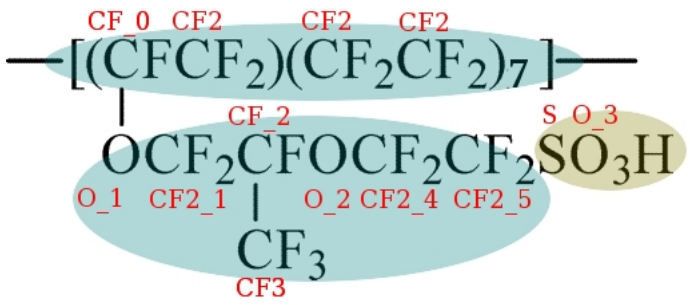

Figure S1: Chemical structure of a segment of a Nafion chain adapted from [19]. Blue ellipses denote hydrophobic portions, while the yellow ellipse denotes the hydrophilic portion. Red labels correspond to distinct particle types in the force field.

S1.2 Non-bonded parameters

Type	q	σ	ϵ
CF3	0.0000	0.46000	6.56843
CF2	0.0000	0.46000	2.49434
CF_0	0.1577	0.44500	0.24943
CF2_1	-0.0046	0.44500	0.24943
CF_2	0.2097	0.44500	0.24943
CF2_4	-0.0106	0.44500	0.24943
CF2_5	-0.3340	0.44500	0.24943
O_1	-0.2742	0.30700	0.71170
O_2	-0.2604	0.30700	0.71170
S	1.4124	0.35500	1.04650
O_3	-0.6320	0.31500	0.83720
ON	-0.5540	0.31507	0.63627
HN	0.5180	0.00000	0.00000
IW	-1.1128	0.00000	0.00000
OWT4	0.0000	0.31589	0.77490
HW	0.5564	0.00000	0.00000

Table S1: Non-bonded parameters. σ and ϵ are Lennard-Jones parameters in units of nm and kJ/mol, respectively. q's are partial charges in units of e, the elementary charge. Optimized cross-interactions for combinations OWT4/CF2 and OWT4/CF3 are discussed in Section S1.3.

S1.3 Optimized water/perfluorocarbon interactions

S1.3.1 Potential Models

Although many models have been developed for perfluorocarbons, we restricted the present study to models that have formed the basis of publications involving fuel cell membranes. We might then gain further insight into these publications by better understanding the limitations of the models that underpin them. To that end, we studied the uncharged, united-atom "model-T" model of Cui and coworkers [6], and the fully-atomistic OPLS model of Watkins and Jorgensen [34]. The united-model represents each CF_x groups as a single particle, and the fully-atomistic model explicitly accounts for the fluorines. The intermolecular potentials of both models consist of a Lennard-Jones potential, a harmonic bond-angle bending potential, and a Fourier series dihedral-angle potential. In addition, the fully-atomistic model has electrostatic interactions and a harmonic bond-stretching potential.

Having chosen perfluorocarbon models, we combined these models with different water models and different mixing rules for the Lennard-Jones parameters. In particular, we used the rigid, three-site SPC/E model of Berendsen and coworkers [2], and the rigid, four-site TIP4P/2005 model of Abascal and Vega [1]. To describe the O/CF_x dispersion interaction, we applied the Lorentz-Berthelot (Eqs. S1 and S2) and Kong mixing rules [17] (Eqs. S3 and S4).

$$\sigma_{ij} = \frac{1}{2}(\sigma_{ii} + \sigma_{jj}) \tag{S1}$$

$$\epsilon_{ij} = \sqrt{\epsilon_{ii}\epsilon_{jj}} \tag{S2}$$

$$\sigma_{ij} = \left\{ \frac{\epsilon_{ii}\sigma_{ii}^{12}}{2^{13}\sqrt{\epsilon_{ii}\sigma_{ii}^{6}\epsilon_{jj}\sigma_{jj}^{6}}} \left[1 + \left(\frac{\epsilon_{jj}\sigma_{jj}^{12}}{\epsilon_{ii}\sigma_{ii}^{12}} \right)^{1/13} \right]^{13} \right\}^{1/6} \tag{S3}$$

$$\epsilon_{ij} = \frac{2^{13}\epsilon_{ii}\sigma_{ii}^{6}\epsilon_{jj}\sigma_{jj}^{6}}{\epsilon_{ii}\sigma_{ii}^{12}\left[1 + \left(\frac{\epsilon_{jj}\sigma_{jj}^{12}}{\epsilon_{ii}\sigma_{ii}^{12}} \right)^{1/13} \right]^{13}} \tag{S4}$$

For the fully-atomistic perfluorocarbon model, we only used the TIP4P/2005 water model

and Lorentz-Berthelot mixing rules, since the focus of the present study is obtaining a united-atom perfluorocarbon model that can accurately predict water solubility.

When Lorentz-Berthelot and Kong mixing rules proved to be inadequate, we manually adjusted the C_6 parameter of the Lennard-Jones potential, where

$$U(r_{ij}) = \frac{C_{12}}{r^{12}} - \frac{C_6}{r^6}$$
$$C_{12} = 4\varepsilon_{ij}\sigma_{ij}^{12}$$
$$C_6 = 4\varepsilon_{ij}\sigma_{ij}^{6}$$

C_6 can be thought of as the attractive parameter of the Lennard-Jones potential, while C_{12} is the repulsive parameter.

S1.3.2 Simulation Methodology

We computed the mole fraction of water (1) in perfluorohexane (2) by considering a system of a water-rich phase in equilibrium with a perfluorohexane-rich phase, as was done to obtain the experimental data. By equating the fugacity of water in each phase, we find that:

$$x_1^\alpha = \frac{P_1^{sat}}{H_1^\alpha} \tag{S5}$$

where P_1^{sat} is saturation pressure of water, taken to be the fugacity of water in the water-rich (β) phase. The fugacity of water in the perfluorohexane-rich (α) phase is $x_1^\alpha H_1^\alpha$, where H_1^α is the Henry's Law constant [29]:

$$\begin{aligned} H_1^\alpha &= \lim_{x_1^\alpha \to 0} \left(\frac{f_1^\alpha}{x_1^\alpha} \right) \\ &= \lim_{x_1^\alpha \to 0} \left[\frac{\rho^\alpha}{\beta} \exp\left(\beta \mu_1^{ex,\alpha}\right) \right] \end{aligned} \tag{S6}$$

where $\beta = RT$. We calculated $\mu_1^{ex,\alpha}$ using the test-particle insertion technique [35], according to which

$$\mu_1^{ex,\alpha} = -\frac{1}{\beta} \ln \left(\frac{\langle \overline{V \exp(-\beta \Delta\phi)} \rangle}{\langle V \rangle} \right) \tag{S7}$$

where V is the volume and $\Delta\phi$ is the interaction energy between the test-particle/test-molecule and the rest of the system. The overbar denotes an average over multiple insertions into a single configuration, whereas the brackets denote an average over the ensemble of configurations.

In order to compute the ensemble average in Eq. S7, we used the molecular dynamics (MD) technique to generate a set of configurations of pure perfluorohexane for each solubitily calcution. Starting from equilibrated configurations, we performed NPT MD production runs for 4 ns with a 2 fs timestep for the united-atom model and a 0.5 fs timestep for the fully atomistic model. We maintained the temperature at a fixed value with the Nose-Hoover thermostat [24, 15] and the pressure with Parrinello-Rahman barostat [26, 25]. For the united-atom perfluorocarbon model, we maintained constant bond lengths using the LINCS algorithm [12].

After generating the sets of configurations, we inserted water molecules 1000-250000 times at random locations and orientations within each configuration and recored the energies. After each test-particle insertion run, we plotted the scaled distribution of insertion energies to verify that we had performed enough insertions. Figure S2 shows several such distributions, as well as a distribution for test particle insertions of TIP4P/2005 water into TIP4P/2005 water. We performed the last calculations in order to validate the implementation of test-particle insertions we were using. Although this calculation was far more difficult than the perfluorocarbon calculations, requiring $9.12 \cdot 10^{11}$ insertions, we nevertheless obtained an accurate estimate for the fugacity of TIP4P/2005 water, $f_w = 7.89 \pm 0.17$ bar. For comparison, the fugacity of this water model obtained by Vega and coworkers [33] using Gibbs-Duhem integration was 7.39 bar. We would expect the perfluorocarbon calculations to be even more accurate, since the corresponding insertions energies are better sampled, as

shown in Figure S2. For calculations of both water fugacity and water solubility in atomistic perfluorocarbons, we inserted whole water molecules into the system. In the case of the uncharged united-atom model, we inserted only the single Lennard-Jones site centered at the oxygen atom because there are no electrostatic interactions in the system.

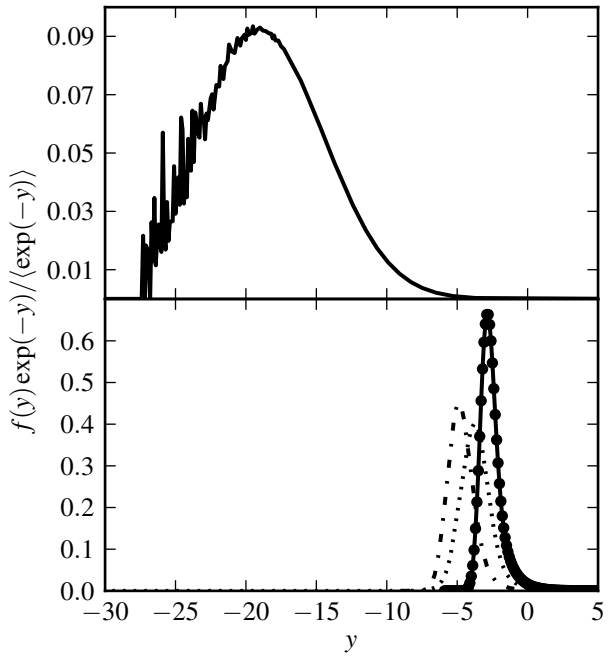

Figure S2: Scaled distribution of test-molecule insertion energies at $T = 298.15$ K, where $y = \beta\Delta\phi - \ln(V/\langle V\rangle)$, $\Delta\phi$ is the insertion energy, V is the volume, and $f(y)$ is the probability density function. Connected circles, TIP4P/2005 water in UA perfluorohexane with Lorentz-Berthelot mixing rules; dot-dash line, with optimized C_6 parameters. Dotted line, TIP4P/2005 water in atomistic perfluorohexane with Lorentz-Berthelot mixing rules. Solid line, TIP4P/2005 water in TIP4P/2005 water.

We used the recorded energies of the insertions to compute the Henry's Law constant according to Eqs. S6 and S7. We then related the Henry's Law constant to the mole fraction using Eq. S5, taking P_1^{sat} to be the vapor pressure of the water models rather than the the experimental vapor pressure. We estimated these vapor pressures by fitting the Antoine Equation [29] to data from Vega and coworkers [33] in the case of TIP4P/2005 and from Boulougouris and coworkers [3] in the case of SPC/E.

To estimate the uncertainty u of the mole fractions, we first calculated the uncertainty

u' of $\langle V \exp(-\beta\Delta\phi)\rangle$ using the method of Flyvbjerg and Petersen [10]. We then related u' to u using Eqs. S5, S6, and S7:

$$u = \frac{\beta P_1^{sat}}{N} u'$$

where N is the number of molecules in the system.

We performed both molecular dynamics runs and test-particle insertion runs with the Gromacs molecular dynamics package version 4.5.1 [13]. We truncated van der Waals interactions at 1.15 nm for the united-atom model and 1.0 nm for the atomistic model. We also shifted and smoothed the van der Waals interactions according to the formula in the Gromacs manual [32] so that both the energy and force are continuous. We applied the corresponding analytical long-range corrections to the energy and pressure given in the manual. In addition to approximating long-range interactions beyond the cut-off, these analytical expressions also correct for the shifting and smoothing of the Lennard-Jones potential.

To account for the long-range electrostatic interactions in the atomistic model, we used the Smooth Particle Mesh Ewald technique [9]. We truncated the real-space contribution at 0.9 nm, and use a grid-spacing of 0.1 nm for the Fourier-space contribution with cubic interpolation. We set β to be 3.12 nm^{-1}, where β determines the width of the Gaussian.

S1.3.3 Water solubility in perfluorohexane

All of the combinations of perfluorocarbon models, water models, and mixing rules systematically under-predicted the solubility of water in perfluorohexane but still followed the correct qualitative trend, as Figure S3 shows. Looking at Table S2, it is clear that the average deviations from experiment for each model combination are all around -90%, with the best performing combinations being united-atom perfluorocarbons with Lorentz-Berthelot mixing rules and either of the water models. For comparison, the united-atom model for hexane tested by Boulougouris and coworkers [4] systematically overpredicts the Henry's Law constant of water in the polymer-rich phase, but by a much smaller margin. One explanation for the poorer performance of the united-atom model for perfluorocarbons may be that the

model does not reproduce pure-component coexistence densities as well as the hexane model. The coexistence density not only determines the free volume available for insertions, but also the strength of dispersion and electrostatic interactions between the test-molecule and the system. It is also plausible that neglecting electrostatics is a worse approximation in the case of perfluorocarbons, because the C-F bond has a higher dipole moment (1.41 D) than the C-H bond (0.4 D) due to the high electronegativity of the fluorine atom (3.98) compared to the hydrogen atom (2.20) [14]. However, if we correct for these two shortcomings of the united-atom model by using a more accurate, fully atomistic model, the agreement with experiment actually becomes slightly *worse*, as Table S2 indicates. Therefore, at least part of the error must come from a source that is common to all of these model combinations.

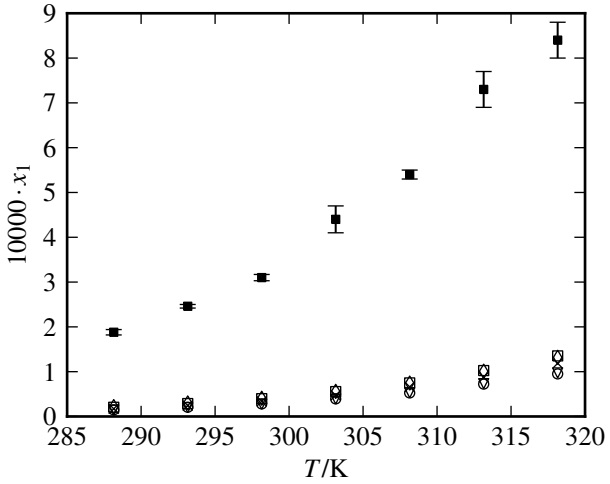

Figure S3: x_1^α, mole fraction of water in the perfluorocarbon-rich phase of the water (1) + perfluorohexane (2) system at $p = 0.1$ MPa. □, TIP4P/2005 water in UA perfluorohexane with Lorentz-Berthelot mixing rules; ▽, with Kong mixing rules. ×, TIP4P/2005 water in atomistic perfluorohexane with Lorentz Berthelot mixing rules. ◊, SPC/E water in UA perfluorohexane with Lorentz-Berthelot mixing rules; ◯, with Kong mixing rules. ■, experimental data [11].

Solute	Solvent	Mixing Rule	$100 \cdot \Delta x_1^\alpha / x_1^\alpha$	T/K = 288.15		T/K = 318.15	
				$10000 \cdot x_1^\alpha$	$\pm 10000 \cdot u$	$10000 \cdot x_1^\alpha$	$\pm 10000 \cdot u$
TIP4P/2005	UA PFH	LB	-87	0.2056	0.0003	1.3521	0.0021
TIP4P/2005	UA PFH	Kong	-91	0.1394	0.0002	0.9719	0.0013
TIP4P/2005	atom. PFH	LB	-89	0.1717	0.0011	1.1858	0.0083
SPC/E	UA PFH	LB	-87	0.2190	0.0003	1.3194	0.0018
SPC/E	UA PFH	Kong	-91	0.1488	0.0002	0.9504	0.0013
TIP4P/2005	UA PFH	Optimized	-0.74	1.8379	0.0017	8.7540	0.0084

Table S2: x_1^α, mole fraction of water in the perfluorocarbon-rich phase of the water (1) + perfluorohexane (2) system at $p = 0.1$ MPa. $\Delta x_1^\alpha / x_1^\alpha$ is the average fractional deviation of the mole fraction from experiments for each data series. u is the estimated uncertainty in x_1^α. We show only the first and last data points from each data series; the full data set can be found in the Supporting Information.

If we compare the two best performing combinations with experiments in terms of the different quantities in Eq. S5, we find that neither water model accurately predicts the vapor pressure, thereby introducing substantial error into the calculation of the mole fraction. In fact, Table S3 shows that the simulations actually produce Henry's Law constants of roughly the correct order of magnitude, despite the mole fraction being an order of magnitude too low. While it is tempting to choose a water model that more accurately describes the vapor face, this choice would likely be made at the expense of the liquid and solid phase properties. It is difficult to devise an accurate model of all three phases of water without including polarizability and three-body terms, as Vega and coworkers explain [33]. This added complexity would be an unacceptable computational burden for large-scale simulations of perfluorocarbons and their derivatives. Therefore, we will refrain from changing the water models.

	$10000 \cdot x_1^\alpha$	$100000 \cdot P_1^{sat}$/bar	H_1^α/bar
Experiments [11]	1.88	1704	90.6
TIP4P/2005	0.2056	339.9	165.4
SPC/E	0.2190	454.6	207.6

Table S3: Solubility properties of the the water (1) + perfluorohexane (2) system. Mole fraction of water x_1^α in the perfluorocarbon-rich phase, vapor pressure of water P_1^{sat}, and Henry's constant of water in the perfluorohexane-rich phase H_1^α. $T = 288.15$ K and $p = 1.0$ bar. We modeled perfluorohexane with the united-atom potential of Cui and coworkers [6], and water with the TIP4P/2005 potential or SCP/E potential as indicated.

Another potential source of error that would be common to all models is inadequate mixing rules for the Lennard-Jones parameters, since both perfluorocarbon models were parameterized to reproduce only pure component properties. Neither the Lorenz-Berthelot rules nor the Kong rules are gaurunteed to give good predictions of mutual solubilities of components with large differences in polarity, as Potoff and coworkers demonstrated [27]. This observation may help explain why Lorenz-Berthelot mixing rules give relatively accurate predictions of the solubility of non-polar oxygen in perfluorohexane that deviate only 30% from experiments, as Costa Gomes and Padua reported [5]. These authors used the same atomistic perfluorocarbon model as we did in the present study, though they also used an oxygen model that reproduces vapor pressures to within only 8.3% of experiments [20], further improving the accuracy. Given that these mixing rules are inadequate for predicting water solubilty, one solution would be to use polarizable models, but as we noted previously, this would add a significant computational cost to the simulations. Instead, we can correct the problem while avoiding additional computional burden and preserving the pure phase properties of the models by simply adjusting the unlike parameters on an empirical basis. We optimized the parameters for only the system of united-atom perfluorocarbon and TIP4P/2005 water since the objective of the present study is to find an accurate united-atom perfluorocarbon model. In particular, we increased the C_6 parameter for the O/CF_x dispersion interaction by varying amounts until we found that multiplying C_6 by 1.35 gave excellent agreement with experiments. Figure S4 illustrates this process, and Table S2 in-

dicates that the deviation from experiments for the optimized mixing parameters is only -0.74%.

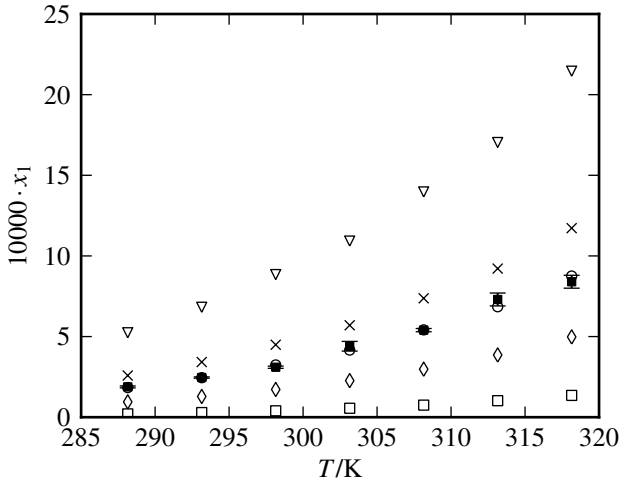

Figure S4: x_1^α, mole fraction of water in the perfluorocarbon-rich phase of the water (1) + perfluorohexane (2) system at $p = 0.1$ MPa. In every simulation, we inserted TIP4P/2005 water into UA perfluorohexane. □, original C_6 parameter; ◊, C_6 that is 1.25 times the original value; ▽, C_6 that is 1.5 times the original value; ◯, C_6 that is 1.35 times the original value; ×, C_6 that is 1.4 times the original value; ■, experimental data [11].

S1.4 Bond potentials

The potential energy for bonded interactions is computed using the following function:

$$V = \frac{1}{2}k(r - r_0)^2$$

Parameters for the function can be found in Table S4. All water molecules are completely rigid.

Type 1	Type 2	r_0	k
CF3	CF2	0.1540	–
CF2	CF2	0.1540	–
CF_0	CF3	0.1540	–
CF_0	CF2	0.1540	–
CF_0	CF2_1	0.1602	259408
CF3	CF_2	0.1602	259408
CF2_1	CF_2	0.1602	259408
CF2_4	CF2_5	0.1602	259408
CF_0	O_1	0.1380	267776
CF2_1	O_1	0.1380	267776
CF_2	O_2	0.1380	267776
CF2_4	O_2	0.1380	267776
S	O_3	0.1490	572103
S	CF2_5	0.1800	192708
ON	HN	0.0957	462750

Table S4: Parameters for bond potentials. r_0 and k are in units of nm and kJ/mol/nm^2, respectively. A "–" entry for k indicates that the bond is rigid.

S1.5 Angle potentials

The potential energy for angle-bending interactions is computed using the following function:

$$V = \frac{1}{2}k(\theta - \theta_0)^2$$

Parameters for the function can be found in Table S5. All water molecules are completely rigid.

Type 1	Type 2	Type 3	θ_0	k
CF3	CF2	CF2	114.60	519.655
CF2	CF2	CF2	114.60	519.655
CF3	CF2	CF3	114.60	519.655
CF2	CF_0	CF3	114.60	519.655
CF2	CF_0	CF2	114.60	519.655
CF_0	CF2	CF2	114.60	519.655
CF2	CF_0	O_1	109.50	418.400
CF3	CF_0	O_1	109.50	418.400
CF_0	O_1	CF2_1	109.50	502.080
O_1	CF2_1	CF_2	109.50	418.400
CF2_1	CF_2	CF3	109.60	334.720
CF2_1	CF_2	O_2	109.50	418.400
CF3	CF_2	O_2	109.50	418.400
CF_2	O_2	CF2_4	109.50	502.080
O_2	CF2_4	CF2_5	109.50	418.400
CF2_4	CF2_5	S	112.60	418.400
CF2_5	S	O_3	106.75	1248.37
O_3	S	O_3	115.00	1386.05
HN	ON	HN	104.52	836.8

Table S5: Parameters for angle-bending potentials. θ_0 and k are in units of degrees and kJ/mol/rad^2, respectively.

S1.6 Dihedral potentials

The potential energy for dihedral angle bending interactions is computed using either of the following function:

$$V = \sum_{i=1}^{4} C_i[1 + (-1)^{i-1}\cos(i\phi)] \tag{S8}$$

$$V = \sum_{i=1}^{8} C_i \cos^{i-1}\psi \tag{S9}$$

where $\psi = \phi - 180$. $\phi = 0$ corresponds to the *cis* configuration. Parameters for both functions can be found in Table S6.

Type 1	Type 2	Type 3	Type 4	C_1	C_2	C_3	C_4	C_5	C_6	C_7	C_8
CF2	CF2	CF_0	O_1	-17.84	6.36	28.08	0.0	–	–	–	–
CF2	CF_0	O_1	CF2_1	4.92	-16.26	11.96	0.0	–	–	–	–
CF3	CF_0	O_1	CF2_1	4.92	-16.26	11.96	0.0	–	–	–	–
CF_0	O_1	CF2_1	CF_2	4.92	-16.26	11.96	0.0	–	–	–	–
O_1	CF2_1	CF_2	CF3	-17.84	6.36	28.08	0.0	–	–	–	–
O_1	CF2_1	CF_2	O_2	-17.82	5.76	26.62	0.0	–	–	–	–
CF2_1	CF_2	O_2	CF2_4	4.92	-16.26	11.96	0.0	–	–	–	–
CF3	CF_2	O_2	CF2_4	4.92	-16.26	11.96	0.0	–	–	–	–
CF_2	O_2	CF2_4	CF2_5	4.92	-16.26	11.96	0.0	–	–	–	–
O_2	CF2_4	CF2_5	S	25.21	5.155	11.96	0.0	–	–	–	–
CF2_4	CF2_5	S	O_3	0.0	0.0	5.777	0.0	–	–	–	–
CF3	CF2	CF2	CF2	4.950	-2.351	11.268	56.538	-65.479	-117.799	76.607	34.286
CF2	CF2	CF2	CF2	4.950	-2.351	11.268	56.538	-65.479	-117.799	76.607	34.286
CF2	CF_0	CF2	CF2	4.950	-2.351	11.268	56.538	-65.479	-117.799	76.607	34.286
CF3	CF_0	CF2	CF2	4.950	-2.351	11.268	56.538	-65.479	-117.799	76.607	34.286
CF_0	CF2	CF2	CF2	4.950	-2.351	11.268	56.538	-65.479	-117.799	76.607	34.286

Table S6: Parameters for dihedral angle bending potentials. C_i's are in units of kJ/mol. Dihedral angles with only four parameters are modeled with Eq. S8; those with eight parameters are modeled with Eq. S9.

S2 Density

Densities are reported in Figure S5. Although our model systematically overpredicts the density of Nafion, it has the same slope, indicating that like experiments[36], it exhibits nearly zero volume of mixing. Therefore, the error in the simulations comes from the density of the dry polymer. This error in the dry polymer density likely comes from the united-atom perfluoroalkane model, which is known to deviate from experimental densities by ca. 10% for perfluoropentane[6]. Other models from the simulation literature predict densities that are closer to experiments, however their behavior with respect to hydration deviates from experiments.

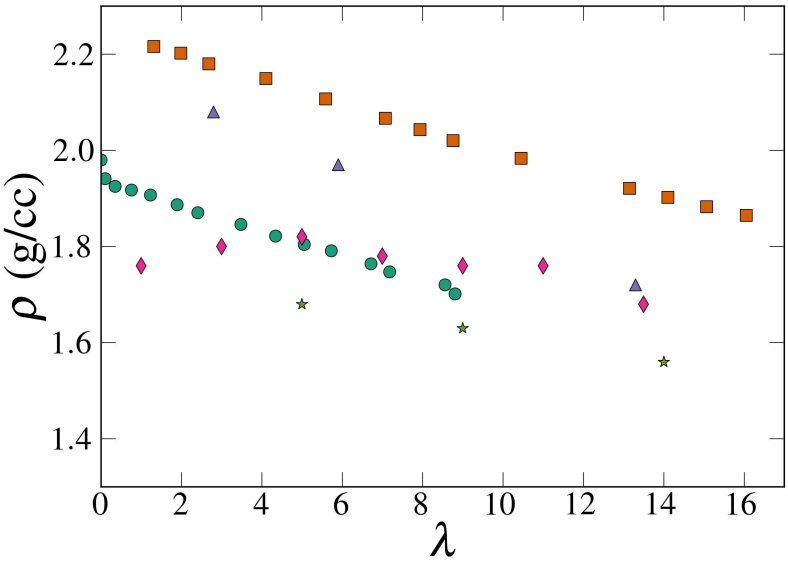

Figure S5: Density of Nafion as a function of hydration. ●: experimental data at 353 K from Zhao et al.[36] ■: our simulation data at 353 K ▲: simulation data of Urata et al.[31] at 358 K. ♦: simulation data of Devanathan et al.[7] at 300 K. ★: simulation data of Voth et al.[30] at 353 K.

S3 S/O(H_3O^+) RDF

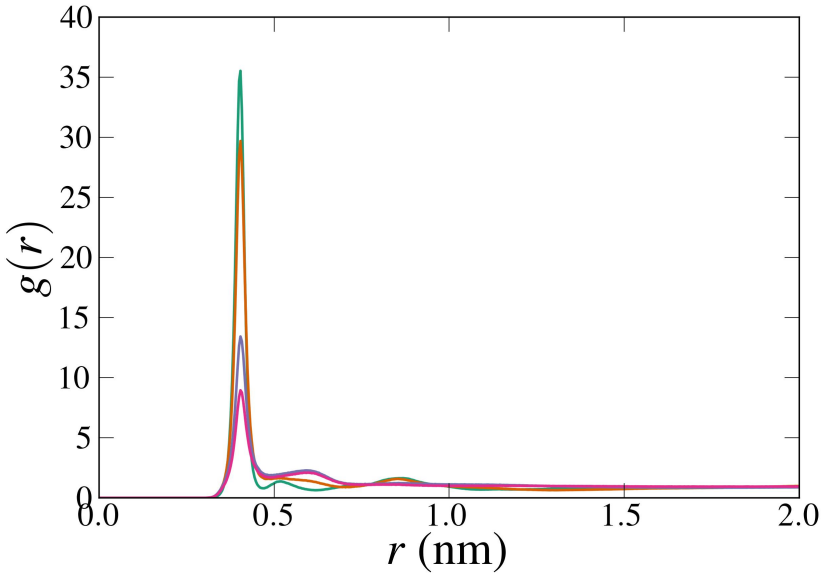

Figure S6: Pair correlation function for pairs of sulfur and oxygen (H_3O^+) as a function of hydration at 353 K. The height of the first peak decreases with hydration. Hydration levels shown: $\lambda = 1.3, 2.7, 8.8, 16$.

S4 Effects of chain length on sorption isotherm

The majority of the simulations in Figure S9 were equilibrated using the procedure described in Section 2 of the manuscript, in which molecules were placed far away from one another in an extremely large box, and the box was compressed using NPT molecular dynamics. In light of recent work by Lucid et al.[18] that shows that long chains are difficult to equilibrate, two additional simulations were performed for chains with 24 monomers to verify that these simulations were equilibrated with respect to water activity.

For the first simulation, the initial configuration was prepared by starting with an equilibrated configuration at low hydration ($\lambda = 1.3$) (see Figure S7), and suddenly inserting enough water to bring it to the target hydration level ($\lambda = 7.1$). Water was inserted by first making the chains whole across the periodic boundaries, enlarging the box in one dimension,

inserting the water, and then finally applying the periodic boundary conditions so that all the coordinates are inside the box again. This procedure ensures that the conformations of the chains are left unchanged. The resulting configuration is shown in Figure S8.

For the second simulation, the initial configuration was prepared by starting with an equilibrated configuration at high hydration ($\lambda = 20$), and suddenly deleting enough water to bring it to the target hydration level. As in the up-jump case, the conformations of the chains were left unchanged. After the abrupt changes in hydration, both the up-jump and the down-jump simulations were equilibrated for at least 15 ns.

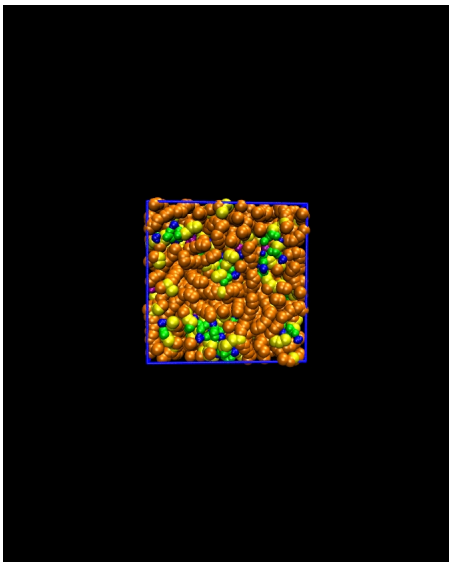

Figure S7: Initial configuration for the "up-jump" simulations before water is added to bring it to the target hydration level. Purple particles belong to the water molecules, while the orange particles belong to the polymer backbone.

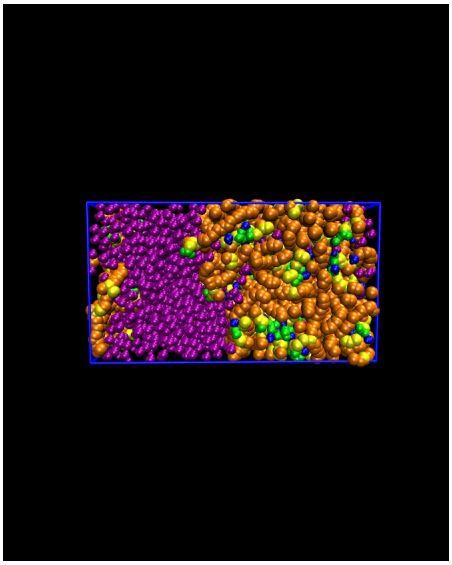

Figure S8: Initial configuration for the "up-jump" simulations after water is added to bring it to the target hydration level. Purple particles belong to the water molecules, while the orange particles belong to the polymer backbone.

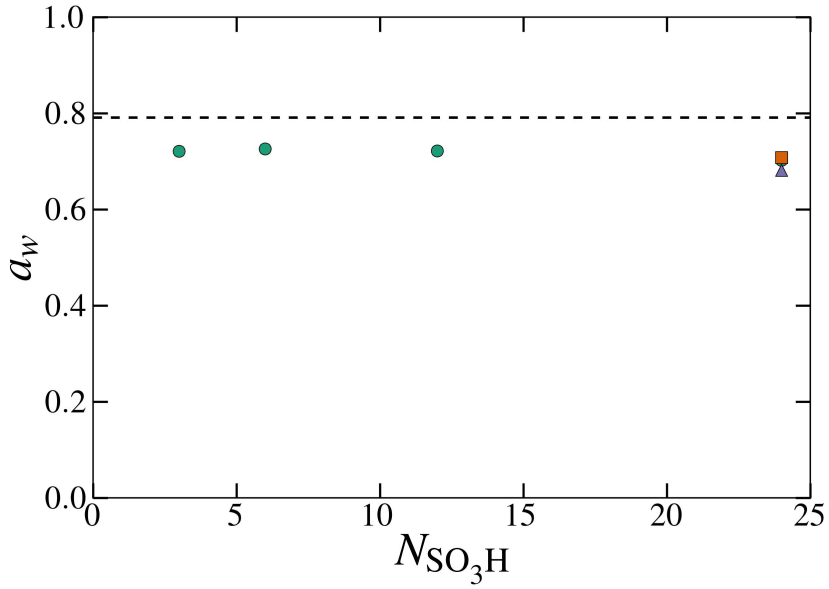

Figure S9: Water activity as a function of chain length for hydration level of $\lambda = 7.07$ and an overall number of sulfonates fixed at 192. Chain length is reported as the number of sulfonates per chain, N_{SO_3H}. The dashed line is the experimental activity at this hydration level [36]. ●: simulations equilibrated using the procedure described in Section 2 of the manuscript. ■: simulations equilibrated using the "up-jump" procedure (see text). ▲: simulations equilibrated using the "down-jump" procedure (see text).

S5 Effects of side chain placement

Since the exact distribution of side chains along the backbone is unknown in experimental Nafion [16], there are many chain structures worth investigating. Such an investigation is beyond the scope of this paper. However, we did test one variation to roughly estimate the sensitivity of our results on chain structure. In particular, we considered the case of chains that are not only equally spaced, but also symmetrically placed along the backbone so that each terminus is the same distance away from a side chain.

Figures S10 and S11 compare radial distribution functions between the asymmetric chain structure we used in the bulk of our simulations, and the symmetric structure discussed above.

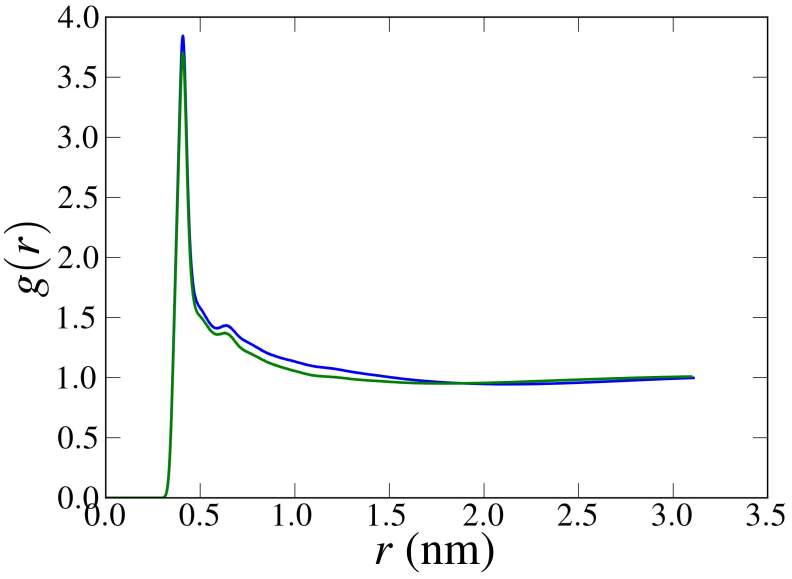

Figure S10: Radial distribution of water/hydronium oxygen atom around a sulfur atom at $\lambda = 16$ and $T = 353$ K. Blue curve: asymmetric chains; green curve: symmetric chains.

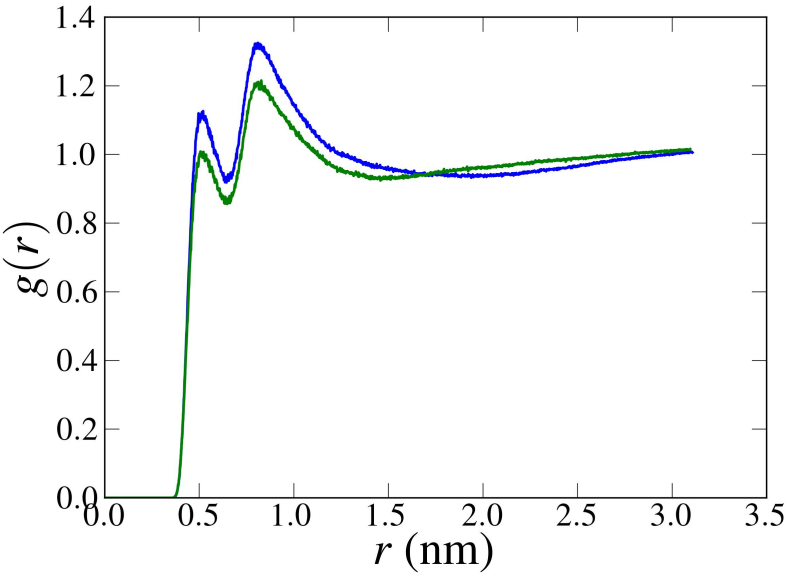

Figure S11: Radial distribution of sulfur atoms around an arbitrary reference sulfur atom at $\lambda = 16$ and $T = 353$ K. Blue curve: asymmetric chains; green curve: symmetric chains.

S6 Heats of sorption

The heats of sorption can be empirically obtained from plots of $\ln 1/f$ versus $1/T$, as shown in Figure S12. They can also be predicted by fitting the sorption isotherms to the DGWC theory [8]. We performed the fitting using the Newton Conjugate-Gradient algorithm [23, 22].

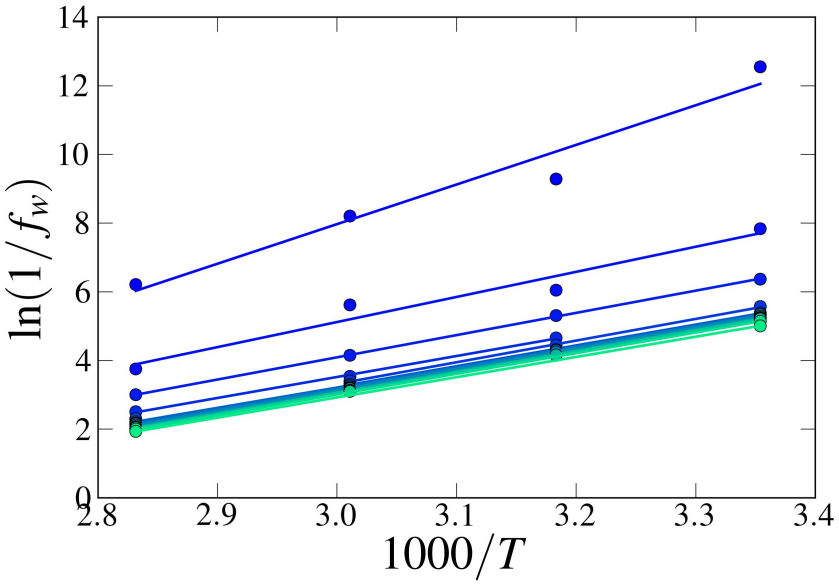

Figure S12: Sorption isotherm data plotted to obtain heats of sorption. Each data set is taken at a fixed λ, with bluer lines indicating lower λ, and greener lines indicating higher λ. A line is fit to each data set, and the slope of the line is taken to be the heat of sorption for the respective value of λ.

S7 Measures of water/hydronium dynamics

λ	τ_{H2O} (ps)	τ_{H3O} (ps)	D_{H2O} (cm^2/s)
1.3	$1.1 \cdot 10^3$		
2.0	$1.4 \cdot 10^2$	$2.9 \cdot 10^4$	
2.7	$4.6 \cdot 10^1$	$2.2 \cdot 10^3$	
4.1	$2.1 \cdot 10^1$	$1.2 \cdot 10^2$	
5.6	$1.3 \cdot 10^1$	$3.0 \cdot 10^1$	$6.3 \cdot 10^{-6}$
7.1	$1.0 \cdot 10^1$	$1.6 \cdot 10^1$	$1.1 \cdot 10^{-5}$
7.9	$9.6 \cdot 10^0$	$1.3 \cdot 10^1$	$9.5 \cdot 10^{-6}$
8.8	$9.0 \cdot 10^0$	$1.1 \cdot 10^1$	$1.3 \cdot 10^{-5}$
10.5	$8.3 \cdot 10^0$	$9.1 \cdot 10^0$	$1.4 \cdot 10^{-5}$
13.2	$7.2 \cdot 10^0$	$7.1 \cdot 10^0$	$1.7 \cdot 10^{-5}$
15.1	$6.9 \cdot 10^0$	$6.4 \cdot 10^0$	$2.2 \cdot 10^{-5}$
16.1	$6.8 \cdot 10^0$	$6.2 \cdot 10^0$	$2.3 \cdot 10^{-5}$
96.3	$4.9 \cdot 10^0$	$3.4 \cdot 10^0$	$4.8 \cdot 10^{-5}$
1570	$2.5 \cdot 10^0$	$3.8 \cdot 10^0$	$6.0 \cdot 10^{-5}$

Table S7: Characteristics times from Figure 10 before normalization. Note that at very high hydration ($\lambda \approx 100$), the characteristic times asymptotically approach their bulk values.

S8 Connolly Surface

To obtain the Connolly surface enclosing hydrophilic particles in the system, we first digitize the hard core volumes of the hydrophilic particles, as shown in Figure S13. Then we perform an operation from mathematical morphology called a binary closing [28] with a spherical structuring element of radius $\sigma_p/2$, where σ_p is the diameter of the probe particle. This operation produces the volume enclosed within the Connolly Surface, as shown in Figure S14. To compute the surface area of this digitized volume, we employ the algorithm from Ref [21].

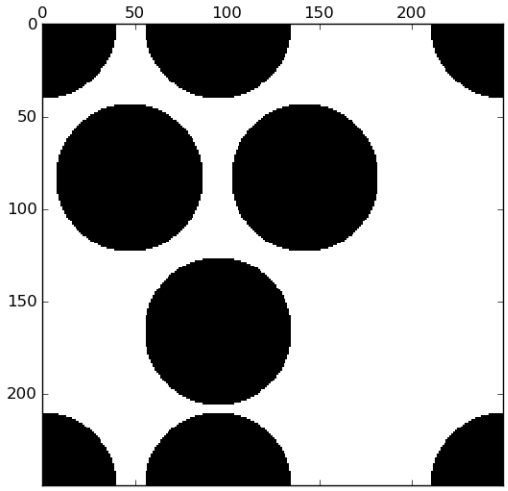

Figure S13: Example 2-D calculation of the Connolly surface and its enclosed volume. This is a digitized image of the volume occupied by particles in the system, where the volume of a particle is defined to be a ball of radius $\sigma/2$ at the particle center and σ is the hard-core diameter from the Lennard-Jones potential.

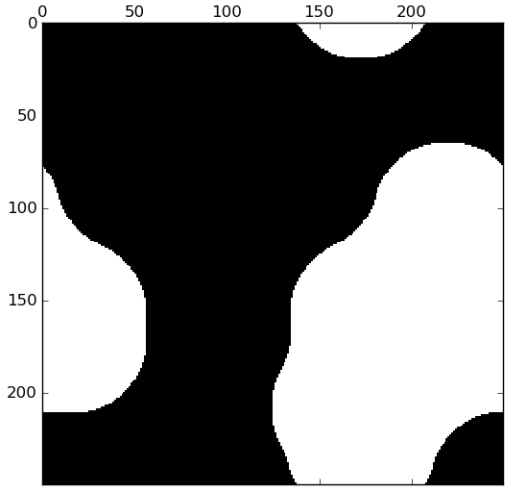

Figure S14: Example 2-D calculation of the Connolly surface and its enclosed volume. This is a digitized image of the volume enclosed within the Connolly surface generated by rolling a probe over the particles in Figure S13. In this case, the radius of the probe is equal to the radius of the particles.

S9 Scaling of the ratio of surface area to volume

Swelling	3-D	2-D	1-D
Example	Spheres	Rods	Lamellae
V	r^3	r^2L	rA
S	r^2	rL	A
S/V	r^{-1}	r^{-1}	r^{-1}
S/V	$V^{-1/3}$	$(V/L)^{-1/2}$	$(V/A)^{-1}$
S/V	$\lambda^{-1/3}$	$\lambda^{-1/2}$	λ^{-1}

Table S8: Expected scaling of the ratio surface area to volume, S/V, with water content, λ, for simple morphologies. All example morphologies assume a fixed number of clusters. r is the dimension of the cluster that changes with hydration. L is an arbitrary fixed length, and A is an arbitrary fixed area.

S10 Backbone relaxation times

Figure S15 illustrates how calculations of monomer relaxation time are precise enough to reveal monotonic behavior with respect to water content, yet are still noisy enough to obscure correlations with water relaxation time at high water contents, as shown in figure S16.

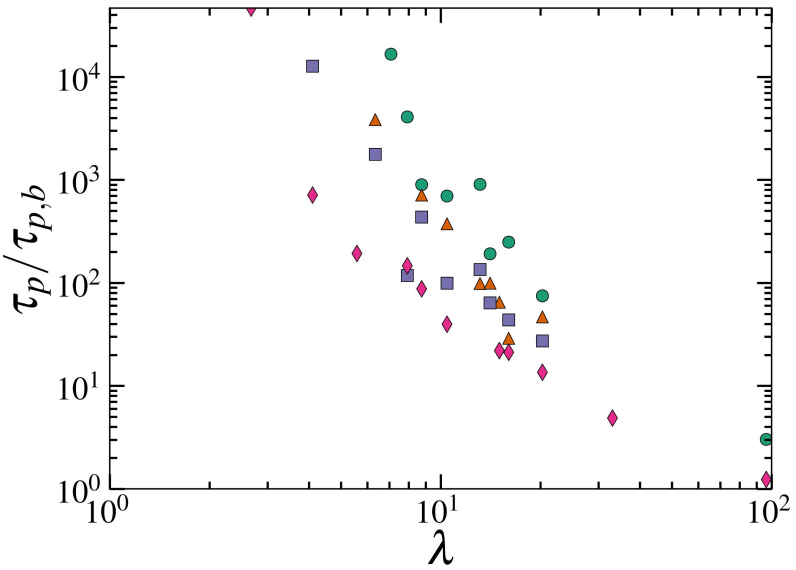

Figure S15: Correlation between water content (λ) and the backbone monomer relaxation time as defined in the main paper at various temperatures. Relaxation times are normalized by their values at the same temperature at infinite dilution. ($\lambda \to \infty$). ●, $T = 298$ K; ▲, $T = 314$ K; ■, $T = 332$ K; ♦, $T = 353$ K.

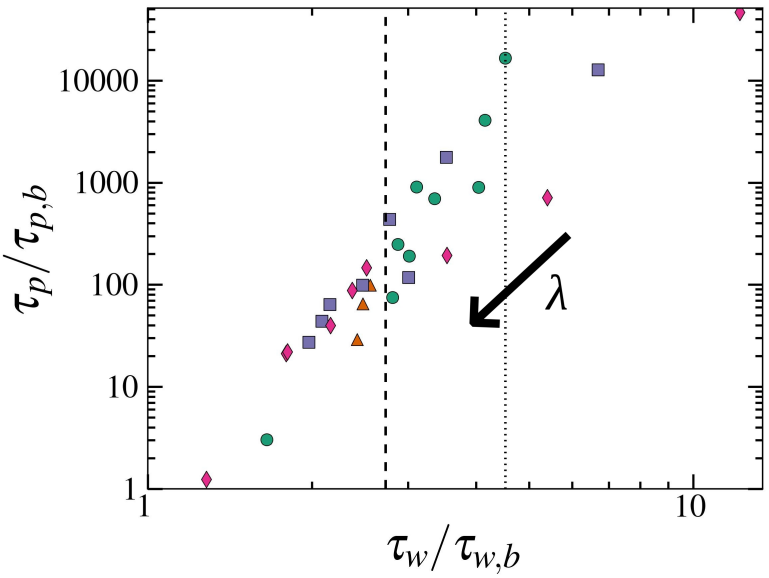

Figure S16: Correlation between the translational relaxation time of water and the backbone monomer relaxation time as defined in the main paper at various temperatures and water contents (λ). Quantities are normalized by their values at the same temperature at infinite dilution. ($\lambda \to \infty$). ●, $T = 298$ K; ▲, $T = 314$ K; ■, $T = 332$ K; ♦, $T = 353$ K. Dashed line marks the value of $\tau_w/\tau_{w,b}$ at which $T = 353$ and SO_3^- groups no longer share water molecules in their first coordination shells (see main paper). Dotted line marks the same quantity at $T = 298$.

References

[1] J. L. F. Abascal and C. Vega. A general purpose model for the condensed phases of water: TIP4P/2005. *The Journal of Chemical Physics*, 123(23):234505, 2005.

[2] H. J. C. Berendsen, J. R. Grigera, and T. P. Straatsma. The missing term in effective pair potentials. *The Journal of Physical Chemistry*, 91(24):6269–6271, November 1987.

[3] Georgios C. Boulougouris, Ioannis G. Economou, and Doros N. Theodorou. Engineering a molecular model for water phase equilibrium over a wide temperature range. *The Journal of Physical Chemistry B*, 102(6):1029–1035, February 1998.

[4] Georgios C. Boulougouris, Jeffrey R. Errington, Ioannis G. Economou, Athanassios Z. Panagiotopoulos, and Doros N. Theodorou. Molecular simulation of phase equilibria for water-n-butane and water-n-hexane mixtures. *The Journal of Physical Chemistry B*, 104(20):4958–4963, May 2000.

[5] Margarida F. Costa Gomes and Agilio A. H. Padua. Interactions of carbon dioxide with liquid fluorocarbons. *The Journal of Physical Chemistry B*, 107(50):14020–14024, December 2003.

[6] S. T. Cui, J. I. Siepmann, H. D. Cochran, and P. T. Cummings. Intermolecular potentials and vapor-liquid phase equilibria of perfluorinated alkanes. *Fluid Phase Equilibria*, 146(1-2):51–61, May 1998.

[7] R. Devanathan, A. Venkatnathan, and M. Dupuis. Atomistic simulation of nafion membrane: I. effect of hydration on membrane nanostructure. *The Journal of Physical Chemistry B*, 111(28):8069–8079, July 2007.

[8] Cari S. Dutcher, Xinlei Ge, Anthony S. Wexler, and Simon L. Clegg. Statistical mechanics of multilayer sorption: Extension of the Brunauer-Emmett-Teller (BET) and

Guggenheim-Anderson-de boer (GAB) adsorption isotherms. *The Journal of Physical Chemistry C*, 115(33):16474–16487, 2011.

[9] U. Essmann, L. Perera, M. L Berkowitz, T. Darden, H. Lee, and L. G Pedersen. A smooth particle mesh ewald method. *Journal of Chemical Physics*, 103(19):8577–8593, 1995.

[10] H. Flyvbjerg. Error estimates on averages of correlated data. *Advances in Computer Simulation*, pages 88–103, 1998.

[11] Mara G. Freire, Lgia Gomes, Lus M. N. B. F. Santos, Isabel M. Marrucho, and Joo A. P. Coutinho. Water solubility in linear fluoroalkanes used in blood substitute formulations. *The Journal of Physical Chemistry B*, 110(45):22923–22929, November 2006.

[12] B. Hess, H. Bekker, H. J.C Berendsen, and J. G.E.M Fraaije. LINCS: a linear constraint solver for molecular simulations. *Journal of Computational Chemistry*, 18(12):1463–1472, 1997.

[13] Berk Hess, Carsten Kutzner, David van der Spoel, and Erik Lindahl. GROMACS 4: Algorithms for highly efficient, load-balanced, and scalable molecular simulation. *Journal of Chemical Theory and Computation*, 4(3):435–447, March 2008.

[14] M. Hird. Fluorinated liquid crystals-properties and applications. *Chem. Soc. Rev.*, 2007.

[15] William G. Hoover. Canonical dynamics: Equilibrium phase-space distributions. *Physical Review A*, 31(3):1695, March 1985.

[16] Seung Soon Jang, Valeria Molinero, Tahir Çagin, and William A. Goddard III. Effect of monomeric sequence on nanostructure and water dynamics in nafion 117. *Solid State Ionics*, 175(1-4):805–808, November 2004.

[17] Chang Lyoul Kong. Combining rules for intermolecular potential parameters. II. rules for the lennard-jones (12-6) potential and the morse potential. *The Journal of Chemical Physics*, 59(5):2464, 1973.

[18] Jeremy Lucid, Simone Meloni, Donal MacKernan, Eckhard Spohr, and Giovanni Ciccotti. Probing the structures of hydrated nafion in different morphologies using temperature-accelerated molecular dynamics simulations. *The Journal of Physical Chemistry C*, 117(2):774–782, January 2013.

[19] Kenneth A. Mauritz and Robert B. Moore. State of understanding of nafion. *Chemical Reviews*, 104(10):4535–4586, October 2004.

[20] Yoshimori Miyano. Molecular simulation with an EOS algorithm for vapor-liquid equilibria of oxygen and ethane. *Fluid Phase Equilibria*, 158-160:29–35, June 1999.

[21] James C Mullikin and Piet W Verbeek. Surface area estimation of digitized planes. *Bioimaging*, 1(1):6–16, March 1993.

[22] Stephen G. Nash. Newton-type minimization via the lanczos method. *SIAM Journal on Numerical Analysis*, 21(4):770–788, 1984.

[23] Jorge Nocedal and Stephen J. Wright. *Numerical Optimization*. Springer, October 2006.

[24] S. Nosé. A unified formulation of the constant temperature molecular dynamics methods. *The Journal of Chemical Physics*, 81:511, 1984.

[25] S. Nos and M. L. Klein. Constant pressure molecular dynamics for molecular systems. *Molecular Physics*, 50(5):1055–1076, 1983.

[26] M. Parrinello. Polymorphic transitions in single crystals: A new molecular dynamics method. *Journal of Applied Physics*, 52(12):7182, 1981.

[27] J.J. POTOFF, J.R. ERRINGTON, and A.Z. PANAGIOTOPOULOS. Molecular simulation of phase equilibria for mixtures of polar and non-polar components. *Molecular*

Physics: An International Journal at the Interface Between Chemistry and Physics, 97(10):1073, 1999.

[28] Frank Y. Shih. *Image Processing and Mathematical Morphology: Fundamentals and Applications*. CRC Press, March 2009.

[29] J. M. Smith, H. C. Van Ness, and M. M. Abbott. *Introduction to Chemical Engineering Thermodynamics*. McGraw-Hill, New York, seventh edition, 1996.

[30] Ying-Lung Steve Tse, Andrew M. Herring, Kwiseon Kim, and Gregory A. Voth. Molecular dynamics simulations of proton transport in 3M and nafion perfluorosulfonic acid membranes. *The Journal of Physical Chemistry C*, 117(16):8079–8091, April 2013.

[31] Shingo Urata, Jun Irisawa, Akira Takada, Wataru Shinoda, Seiji Tsuzuki, and Masuhiro Mikami. Molecular dynamics simulation of swollen membrane of perfluorinated ionomer. *The Journal of Physical Chemistry B*, 109(9):4269–4278, March 2005.

[32] D. van der Spoel, E. Lindahl, B. Hess, A. R. van Buuren, E. Apol, P. J. Meulenhoff, D. P. Tieleman, A. L. T. M. Sijbers, K. A. Feenstra, R. van Drunen, and H. J. C. Berendsen. Gromacs user manual version 4.5, 2010.

[33] C. Vega, J. L. F. Abascal, and I. Nezbeda. Vapor-liquid equilibria from the triple point up to the critical point for the new generation of TIP4P-like models: TIP4P/Ew, TIP4P/2005, and TIP4P/ice. *The Journal of Chemical Physics*, 125(3):034503, 2006.

[34] Edward K. Watkins and William L. Jorgensen. Perfluoroalkanes: Conformational analysis and liquid-state properties from ab initio and monte carlo calculations. *The Journal of Physical Chemistry A*, 105(16):4118–4125, April 2001.

[35] B. Widom. Some topics in the theory of fluids. *The Journal of Chemical Physics*, 39(11):2808, 1963.

[36] Qiao Zhao, Paul Majsztrik, and Jay Benziger. Diffusion and interfacial transport of water in nafion. *J. Phys. Chem. B*, 115(12):2717–2727, 2011.